Chapter 3
Conventional Electron Microscopy, Cryo-Electron Microscopy and Cryo-Electron Tomography of Viruses

José R. Castón

Abstract Electron microscopy (EM) techniques have been crucial for understanding the structure of biological specimens such as cells, tissues and macromolecular assemblies. Viruses and related viral assemblies are ideal targets for structural studies that help to define essential biological functions. Whereas conventional EM methods use chemical fixation, dehydration, and staining of the specimens, cryo-electron microscopy (cryo-EM) preserves the native hydrated state. Combined with image processing and three-dimensional reconstruction techniques, cryo-EM provides 3D maps of these macromolecular complexes from projection images, at subnanometer to near-atomic resolutions. Cryo-EM is also a major technique in structural biology for dynamic studies of functional complexes, which are often unstable, flexible, scarce or transient in their native environments. As a tool, cryo-EM complements high-resolution techniques such as X-ray diffraction and NMR spectroscopy; these synergistic hybrid approaches provide important new information. Three-dimensional cryo-electron tomography goes further, and allows the study of viruses not only in their physiological state, but also in their natural environment in the cell, thereby bridging structural studies at the molecular and cellular levels.

Keywords Capsid • Cryo-electron microscopy • Cryo-electron tomography • Electron microscopy • Fourier transform • Image processing • Resolution • Three-dimensional reconstruction • Viral macromolecular assembly • Virus

J.R. Castón (✉)
Department of Macromolecular Structure, Centro Nacional de Biotecnología (CSIC), c/Darwin 3, Campus de Cantoblanco, 28049 Madrid, Spain
e-mail: jrcaston@cnb.csic.es

M.G. Mateu (ed.), *Structure and Physics of Viruses: An Integrated Textbook*, Subcellular Biochemistry 68, DOI 10.1007/978-94-007-6552-8_3,

Abbreviations

2D	Two-dimensional, two dimensions
3D	Three-dimensional, three dimensions
3DR	Three-dimensional reconstruction
CCD	Charge-coupled device
cryo-EM	Cryo-electron microscopy
cryo-ET	Cryo-electron tomography
CTF	Contrast transfer function
EM	Electron microscopy, electron microscope
FEG	Field emission gun
FSC	Fourier shell correlation
FT	Fourier transform
SEM	Scanning electron microscopy
SSE	Secondary structure element
TEM	Transmission electron microscopy

3.1 Introduction

Microscopy is probably the technique with the greatest influence in the history of biology. Optical (or light) microscopy was introduced to biology in the seventeenth century by Antoni van Leeuwenhoek, who described bacteria and protozoa using a microscope able to enlarge image size approximately 300 times. Light microscopy uses visible light and a system of lenses to magnify images, providing intuitive information on morphology and general structure of the biological model under study. The end of the nineteenth and beginning of the twentieth centuries saw the discovery of electrons and X rays; both provided new alternatives for the observation of matter and stimulated the development of the electron microscope and the X-ray diffractometer. In 1931, Ernst Ruska and colleagues invented the electron microscope (Ruska obtained the Nobel Prize in Physics in 1986). One of the early micrographs taken in the 1930s was of bacterial viruses or bacteriophages, called "tiny hostile bacteria".

It took 300 years to improve the simple light microscope, but less than 40 years to perfect the electron microscope. With electron microscopy (EM), scientists were provided with a powerful method that extended the range of observable structures far beyond the limits imposed by the physics of visible light. Our understanding of cell structure and tissues is based in numerous EM contributions. As in many other fields in biology, viruses have had a decisive role in the development of EM, as they constitute simplified tools with which to standardize preparation methods in

biological applications. In turn, EM has made outstanding contributions to understand virus structure and its relationship with biological function.

Biological EM might be considered a descriptive technique in its origins. The questions addressed by EM have evolved together with our concept of the molecular reality of the cell [1]. The experience accumulated over many decades in the multidisciplinary field of biology has shown that each molecular event is more than the sum of its parts. This is reflected, for example, in the regulation and integration of physiological signals, currently termed "systems biology". Genomics has provided a complete list of the macromolecules in a cell, which led to structural genomics, which in turn provides the basic principles of the structure of proteins, of DNA and of RNA. The basic cellular entities that carry out fundamental biological processes are nonetheless multiprotein assemblies [2]. These macromolecular complexes (some of which may contain nucleic acids) respond to factors that determine their association, disassembly or signal transmission, leading finally to specific molecular events.

To decipher biological processes, the organization of macromolecules and components of macromolecular complexes must be established. X-ray crystallography (Chap. 4) and nuclear magnetic resonance (NMR) spectroscopy (Chap. 5) have provided the atomic structures of the modules or subunits of these molecular machines. Given the difficulties in producing sufficient amounts of these complexes and in their crystallization, the number of structures of large macromolecular complexes that have been determined at near-atomic resolution (by X-ray crystallography) is limited compared to the number of protein structures available. EM acts as a link between structural cell biology and high-resolution structural molecular biology. Over time, descriptive EM has given way to a quantitative approach [3]. Three-dimensional (3D) density maps can be synthesized from two-dimensional (2D) images, as electron micrographs are 2D projections of the 3D (multi-) macromolecular assembly under study [4]. EM images nonetheless have deficiencies, as the electron microscope is not a perfect instrument. These problems can be reduced by subsequent image processing of the micrographs. This progress is reflected in the relatively large number of biological structures that have been resolved thus far to resolutions in the 3.5–4.5-Å range.

EM facilitates the understanding of an atomic structure in its biological context (at lower resolution), particularly when macromolecular assemblies and the relationships of their components are involved. The frontiers between NMR spectroscopy, X-ray crystallography and EM are becoming diffuse, as they form a smooth continuum for visualizing macromolecular structures [5] (see also Chaps. 4, 5 and 7). The emerging relationship among these approaches is a complementary one that can overcome the limitations of each method alone; for instance, atomic models can be fitted accurately into EM-derived maps of larger assemblies [6] (see Chap. 7). Viruses are excellent models of nanomachines; their capsids and other viral protein assemblies have provided some of the most striking images using this hybrid approach [7]. In addition to structure and assembly, the form of EM termed cryo-electron microscopy (cryo-EM) also allows dynamic studies of complexes, which are often unstable, scarce or transient, in their native environment.

A structural description of a macromolecular assembly in its different functional states facilitates a mechanistic understanding of the corresponding processes [8].

In this chapter, we describe the principles of EM, with examples of its applications to the study of some viruses. Most sections in this chapter outline the basis of 3D cryo-EM (cryo-EM plus image processing), illustrating its potential in the marriage with X-ray crystallography (see also Chap. 7). The powerful technique of 3D cryo-electron tomography (cryo-ET), which allows the study of viruses in their natural environment in the cell, is also described. The examples mentioned may give the reader a perspective as to how this approach can be applied to the study of large viral complexes and allow determination of their overall shape, the location of subunits and domains within them, and identification of conformational changes that accompany intermediates in their functional cycle. Moreover, even today in the age of molecular diagnosis, EM remains a mainstay in detecting the causative organism in outbreaks of new and unusual diseases; EM does not require specific reagents to be able to recognize a pathogenic agent [9].

3.2 Transmission Electron Microscopy of Viruses

3.2.1 Basic Concepts and General Experimental Design

The physical basis of EM is the dual particle-wave nature of the electron and its charge. Electrons can be accelerated by electric fields reaching high velocities and accordingly much shorter associated wavelengths than visible light photons, leading to much improved resolution compared with an optical microscope. Electrons are provided by an emission source, such as a heated tungsten or lanthanum hexaboride filament or, alternatively, by a field emission gun (FEG). A FEG generates a much brighter electron beam with better spatial coherence than a thermal ionic electron source. Electrons are accelerated by high voltage, and focused by electromagnetic lenses (condenser lenses) to make a collimated (highly parallel) beam that interacts with the specimen. The interior of the microscope column must be under a high vacuum system to reduce the frequency of electron collision with gas atoms to negligible levels in the path of the electrons; this system also prevents degradation of the coherence and monochromaticity of the electron beam (Fig. 3.1). The sample is inserted in the column through an airlock.

There are two basic types of electron microscopes, the transmission electron microscope (TEM) and the scanning electron microscope (SEM). TEM projects electrons through a very thin specimen; the beam interacts with the specimen and the transmitted electrons are focused by electromagnetic lenses (objective lens and projector lenses) onto a detector to produce a magnified 2D image of the specimen [10]. The electron beam covers a wide area of the specimen. Detectors are a fluorescent screen, a photographic film or a charge-coupled device (CCD). In addition, direct electron detectors (without scintillators to convert the electrons

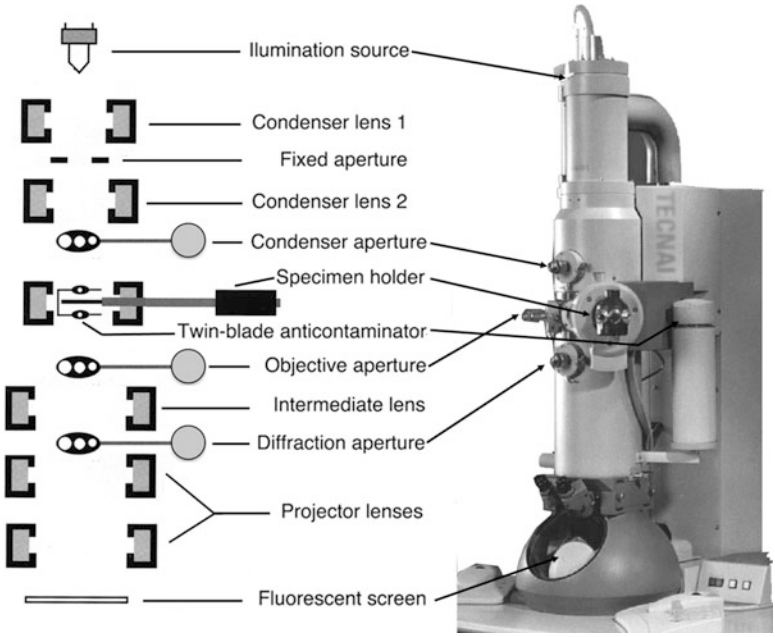

Fig. 3.1 Major components of a transmission electron microscope. Diagram of major components in the column of a modern transmission (cryo-)electron microscope

into photons) are being explored, as they would be superior recording devices for EM images. The brightness of a particular area of the image is proportional to the number of electrons that are transmitted through the specimen.

SEM produces an image that gives the impression of three dimensions. In this microscope, the electron beam is focused to a fine probe and scans the surface of the specimen, point by point, to generate secondary (reflected) electrons from the specimen; these are then detected by a sensor. The image is produced over time as the entire specimen is scanned. There are also scanning transmission electron microscopes (STEM) for analytical use; a scanning beam of electrons penetrates thin samples and provides quantitative determinations of macromolecular masses, and indicates the presence and distribution of the atomic elements in the specimen. The majority of macromolecular (and viral) EM studies are based on TEM.

EM specimens must be solid and thin. Although water is by far the foremost component of living entities, it has long been neglected in EM, as it evaporates in the vacuum of the microscope. Years of research have established many useful procedures for observing biological samples with acceptable structural preservation although their water has been removed (see below). Full preservation of native conformation after complete dehydration nonetheless remains unresolved. Cryo-EM techniques, which began to emerge in the 1980s, consider water as the natural intrinsic component that it actually is. Specimens remain fully hydrated, immobilized in vitreous water (or vitreous ice). Water is cooled very rapidly in

such a way it is solidified without ordering, as it is in hexagonal or cubic ices; the resulting vitreous water is in an amorphous solid state. The specimen is maintained at very low temperature (−170 °C or lower) and the evaporation rate becomes negligible, preserving the hydrated state of the specimen in the microscope [11].

The amount of electron scattering is dependent on specimen density and overall thickness. The specimen must be thin enough to prevent image degradation due to the numerous elastic and inelastic scattering interactions of electrons passing through the specimen [12]. Electrons that interact with the potential field of atomic nuclei usually undergo elastic collisions and are deflected with no loss of energy. They emerge with their wavelength unchanged, but experience an associated phase shift. Elastically scattered and unscattered electrons contribute to image formation. Electrons that interact with the outer electrons of atomic nuclei undergo inelastic collisions and transfer some of their energy to the specimen atoms; this process contributes to image blurring, and is responsible for radiation damage to the specimen. Due to the nonconductive nature of the specimen, these inelastic interactions lead to the formation of many highly reactive ions and free radicals; this results in the breakage of covalent bonds, causing molecular structures to degrade rapidly during observation. Image blurring can be caused by specimen movement, which can include mechanical drift, vibration and/or image thermal drift. These adverse effects can be minimized using imaging strategies in which the electron dose is low [13].

A constant problem with biological specimens is their low contrast, defined as perceptible variation in the intensity between different regions. Two components contribute to contrast, amplitude and phase contrast. Amplitude contrast is due to the corpuscular nature of electrons, and requires use of an objective lens aperture that traps the electrons scattered at large angles (inelastic scattering or high angle elastic scattering). Biological samples scatter electrons weakly (at small angles), and artificial methods are used to enhance scattering properties, such as the introduction of heavy atoms (for example, negative staining). Regions of the specimen that give rise to these trapped electrons appear dark in the image. This mechanism is negligible in unstained specimens. In theory, smaller objective apertures increase the amplitude contrast, but are more prone to astigmatism problems if the aperture is displaced from the center of the beam axis.

Phase contrast is due to the wave-like nature of electrons, and arises from the constructive or destructive interference between the elastically scattered electrons and the unscattered, transmitted electrons. This is the dominant contrast mechanism in cryo-EM of vitrified (unstained) specimens. Elastically scattered electrons experience a phase shift (or difference in path length) as they emerge from the specimen, with no alterations in their amplitude, and this phase shift can be modified. Spherical aberration (inherent to the objective lens of the microscope) and focus setting (directly manipulated by the microscopist) are factors that generate phase contrast. No phase contrast would be seen in an aberration-free microscope when the specimen is imaged exactly in focus (see below).

3.2.2 *Sample Preparation Techniques: Negative Staining, Metal Shadowing, Embedding and Ultramicrotomy*

As important as the development of the electron microscope itself is the development of adequate sample preparation techniques to be used with it. In the late 1950s, detailed images of viruses were obtained by embedding them in a high density (electron-opaque), highly soluble stain, which replicates specimen structure. Heavy metal salts such as phosphotungstic acid, uranyl acetate, and ammonium molybdate have been used successfully as negative stains. Stains stabilize the sample in the harsh conditions necessary for observation, including the hostile atmosphere (high vacuum) and continuous electron irradiation (energy transfer processes). As a general rule, the difficulties associated with biological samples are solved by following four steps: (1) fixation (chemical or physical), (2) dehydration or drying, (3) the introduction of a support (plastic and amorphous carbon layers, resin, metal shadow or vitreous ice), and (4) increase in contrast (heavy, electron-dense elements).

For optimal results, a firm, structureless substrate is essential for specimen support; plastic films such as collodion or formvar stabilized with a thin layer of carbon are appropriate. These films are used as a support in a specimen grid, the electron microscope analog of the glass slide used in light microscopy. EM grids are fine mesh supports (~3 mm in diameter), on which a plastic/carbon film is deposited, and the biological material is adhered for transport and viewing in the electron microscope. Copper is normally used in the fabrication of grids, although other more inert metals such as gold or nickel may be needed.

There are several negative staining procedures; the flotation method is probably the most popular. A plastic/carbon-coated grid is floated on a droplet containing the specimen for 1–3 min to permit adsorption of the specimen. The grids are previously glow-discharged to render the carbon film more hydrophilic and increase specimen adhesion. The grid is then passed through two to three droplets of water, and transferred onto a drop of negative stain for 30–60 s, blotted with filter paper, and air-dried. In principle, the low pH of the negative stain solution, the adsorption of the specimen to the carbon layer, the embedding in a heavy-metal salt cast, as well as the dehydration method can all be expected to severely disrupt the native conformation of the specimen. The technique nonetheless preserves quite well the structure of wide range of specimens, and constitutes a indispensable initial step for higher resolution studies by cryo-EM [14, 15], as resolution is limited by the granularity of the stain to ~20 Å.

The negative staining technique is a very quick and easy method for assessing the homogeneity and quality of many particulate solutions such as purified virus preparations, and requires a minimum of experience and equipment. Limitations are due mainly to structural preservation; stain depicts only the surface features of the specimen and any cavities the stain penetrates, but little or no information is derived about the partially- or unstained internal features. The method is important in

structural virology for fast but unrefined morphological identification. Enveloped viruses are very susceptible to disruption by negative stains and/or air-drying.

Metal shadowing techniques also use heavy metals to enhance the contrast of the low intrinsic electron scattering of biological samples. Shadowing experiments reveal topographic features of specimens by spraying particles of vaporized metal to form a thin coating on whole pre-dried specimens. Fixing and drying of the specimen should preserve the details to be studied; the simplest method is to allow the sample to air-dry, although this technique can result in excessive shrinkage, cracking and/or collapse of fine structures. The freeze-drying method freezes the specimen rapidly while it is still in the aqueous phase. The frozen specimen is transferred to a chamber that maintains a temperature below −80 °C under vacuum, and the solid ice gradually sublimates; preservation is usually better using this process. The freeze-fracture technique replicates fractured surfaces of frozen specimens obtained with a sharp knife; it is especially suited for studies of membrane structure. A variant of this approach is freeze-etching, in which sublimation (etching of ice) is introduced after fracturing.

Platinum or tungsten/tantalum are usually melted and evaporated from a heated electrode, and a second coat of carbon is often used to improve stability of the replica coating. Specimen shadowing can be either unidirectional or rotary. In unidirectional shadowing, the specimen is immobile and is shadowed at an average angle of ~45° in a high vacuum evaporator. This method can be used to measure the height of a specimen from the length of its shadow, and these micrographs are analyzed to obtain topographic maps. In rotary shadowing, the specimen is rotated on a motorized stage and is shadowed from all directions. Metal replicas are released from the underlying biological material by careful chemical treatments such as a hypochlorite solution, and the floating replica is washed thoroughly, carefully fished on fine grids, dried, and then viewed in the microscope.

Embedding and ultramicrotomy of biological samples, including isolated virus particles or a virus-infected tissue or cells, is an elaborate procedure. Specimens are immersed in a matrix that is solidified, then cut into thin slices or sections (50–100 nm thick). The specimen is first chemically fixed to preserve its structure; osmium tetroxide was the first fixative used for EM, but laboratories today use many variations on the fixation process, including potassium permanganate and the standard glutaraldehyde-osmiun tetroxide protocol. The sample is next dehydrated, which consists of the gradual replacement of water with an organic solvent that acts as a "transition solvent" between the aqueous environment of the specimen and the hydrophobic plastic embedding medium; ethanol and acetone are common dehydrating agents. The sample is infiltrated in a resin; in this process, dehydrants are gradually replaced by (viscous) resin monomers such as epoxy mixtures (often called Epon). The resin specimens are transferred into molds or capsules, and placed in an oven in which the epoxy components polymerize to form a solid. There are many types of embedding media with special uses, such as Lowicryl and LR White (acrylic media) used for immunocytochemistry. Finally, the embedded sample is thinly sectioned with a precision (diamond or glass) knife on an

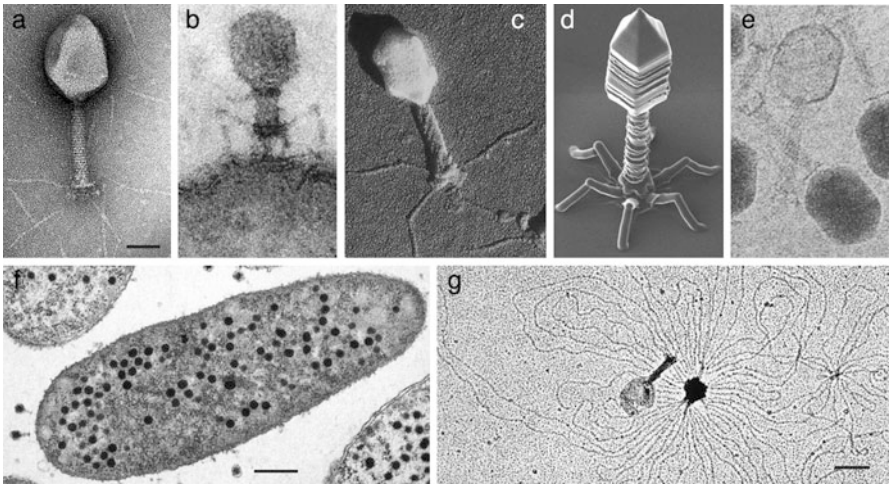

Fig. 3.2 Analysis of bacteriophage T4 by conventional EM and cryo-EM techniques. (**a**) T4 phage negatively stained with 2 % uranyl acetate; darker areas represent local concentrations of stain. The general morphology of the T4 phage, including head, tail, baseplate and fibers can easily be distinguished. The 40.5 Å tail spacing is seen as stacked disks. Note that phage heads are collapsed to different extents, giving the impression of structural heterogeneity due to phage collapse. Bar, 50 nm. (**b**) Thin section showing phage T4 injecting its DNA genome through the bacterial wall; fibers adhere to the outer wall surface and the tail is contracted (Dr. Michel Wurtz, University of Basel, Switzerland; micrograph by J. v.d. Broek). (**c**) Freeze-dried, metal-shadowed phage T4. General morphology is seen as with negative staining, and additional structural details can be inferred: head and tail shadows indicate different heights for these structures; the helical pattern in the tail region is evident in these conditions. (**d**) SEM image of an artificial nano T4 phage fabricated from carbon by focused-ion-beam-induced chemical vapor deposition on a Si surface, about 10× larger than the real virus (micrograph by Reo Kometani and Shinji Matsui, University of Hyogo, Japan). (**e**) Vitrified phage T4; full (*dark*) and empty (*clear*) heads are seen. At this defocus, tail spacing of 40.5 Å is enhanced. (**f**) Thin section through a phage T4-infected *E. coli* bacterium (Dr. Michel Wurtz; micrograph by M. Maeder). Bar, 0.5 μm. (**g**) Air-dried and shadowed broken (by osmotic shock) phage T4 that has released its packaged DNA (Dr. Michel Wurtz; micrograph by J. Meyer). The partially extended DNA indicates high packaging density within the head. Bar, 100 nm

ultramicrotome, sections are picked up on a naked copper grid, and stained with heavy metal salts to enhance contrast.

Bacteriophage T4, of the *Myoviridae* family, is an excellent model that illustrates the complementarity of the information that can be obtained by a variety of conventional TEM procedures (Fig. 3.2). A double-stranded (ds) DNA tailed virus that infects *Escherichia coli*, phage T4 is characterized by a large elongated (prolate icosahedral) capsid (head) (1,150 Å long, 850 Å wide), a tail made of two concentric protein cylinders (1,000 Å long, 210 Å wide), and a complex base plate (460 Å diameter) with six long tail fibers attached to it (1,450 Å long). It is approximately 200 nm long and 80–100 nm wide. The tail is surrounded by a contractile sheath, with helical symmetry (with a pitch of 40.5 Å), which contracts

during infection of the bacterium. dsDNA is densely packaged, ~24 Å interstrand spacings, inside the head [16].

3.2.3 Sample Preparation Techniques: Freeze-Substitution, High Pressure Freezing, and Cryo-Ultramicrotomy

The high vacuum required in the electron microscope column does not allow visualization of living cells in liquid water but, as discussed above, specimen ultrastructure is altered as soon as water is removed. The approaches described thus far increase the stability of dehydrated biological samples by introducing chemical fixatives such as a negative stain agent or osmium tetroxide. As we will see below, the closest approach to the native state is the vitrification of the biological material. This approach is restricted to "thin" structures (viruses are ideal samples), which can be cryo-fixed on a specimen grid by plunge-freezing (rapid immersion in a cryogenic liquid; see below). Thick samples (100–300 μm) can be cryo-fixed by high-pressure freezing.

Freeze-substitution is a low-temperature dehydration method; it can be considered a hybrid technique that bridges the gap between cryo-EM and conventional EM. To ensure good structural preservation, biological samples are cryo-fixed, for example, by high-pressure freezing (see below). They are then freeze-substituted, which consists of dehydration at −90 °C by replacing ice with an organic solvent based on acetone, ethanol or methanol and, if desired, chemical fixatives. After dehydration (or substitution), the temperature is raised to −40 °C to −30 °C and the sample is resin-embedded. Cryo-fixation by high-pressure freezing provides excellent preservation of cellular and molecular architecture for samples between 100 μm and 300 μm thick. This approach has provided realistic views of the crowded eukaryotic cytoplasm, in which protein concentration is ~300 mg/ml.

High-pressure freezing is an approach that permits optimal preservation of biological ultrastructure by cryo-fixation, provided the biological material is not destroyed by water crystallization. This requires high cooling rates (higher than 10,000 K/s) at atmospheric pressure (~1 bar). The native structure is well preserved by conventional freezing (or vitrification) of specimens up to 0.5 μm. Thicker specimens (up to 30 μm) can be frozen without visible ice crystal damage using antifreezing (cryoprotectant) agents, but chemical fixatives are needed; this implies deviation of the native structure and, therefore, loss of high resolution details. Thicker samples (~200 μm) can be adequately frozen under high pressure (~2,000 bars), in which physical properties of water are changed (high pressure is, in fact, a physical cryoprotectant that prevents ice nucleation and crystal growth and increases the depth of vitrification).

Material embedded in vitreous ice is ideal for cutting directly into ultrathin cryo-sections (with a cryo-ultramicrotome using diamond knives) and can be observed in a cryo-electron microscope at liquid nitrogen temperatures, although

cutting-induced deformations and artifacts are a serious problem. This approach is known as cryo-EM of vitreous sections (CEMOVIS). A three-dimensional reconstruction of the specimen in the cryo-section (200 nm thick) can be generated by computerized cryo-ET. CEMOVIS is the best method for preserving whole cells and tissues in their native state, and relatively high resolution is achievable [17].

3.3 Cryo-Electron Microscopy of Viruses

3.3.1 Basic Concepts and General Experimental Design

In cryo-EM of viruses (and other types of biological macromolecular assemblies), the specimen is not dehydrated; instead, it is included in a thin film of water (~0.2 μm or less) that is vitrified [18]. An aliquot of a virus suspension is placed on a grid coated with a holey carbon support film. Excess sample solution is blotted away with filter paper, leaving a very thin film (up to several thousand Å) of virus suspension on the grid, which is rapidly plunged into a cryogen (such as ethane slush) at liquid nitrogen temperature. Freezing is so rapid that water molecules are immobilized in an amorphous state, so-called vitreous or glass-like ice, avoiding physical damage of the specimen by ice crystal formation (Fig. 3.2e). This method provides a natural water-like environment for the virus particle, with no staining or fixing artifacts, and the native structure is preserved with structural integrity near atomic resolution. To avoid devitrification of the sample, the grid bearing the virus sample is maintained at liquid nitrogen temperatures while it is introduced in the microscope with a specimen cryoholder, and for several hours for the recording of micrographs. Alternatively, the grids can be stored indefinitely in liquid nitrogen. Heat transfer between the cryoholder and the microscope can be a serious problem and cause the specimen to vibrate (a result of liquid nitrogen boiling in the cryoholder dewar). Mechanical drift can be another obstacle when the cryoholder is not stably inserted in the column (the specimen must not move by more than a few Å during a 0.5–1 s exposure).

At approximately −170 °C, ice does not sublimate at a significant rate, even in the high vacuum of the electron microscope. Transfer steps must be very rapid to minimize contamination by deposition of hoarfrost (from water vapor), and the cryoholder and the interior of the microscope column are equipped with a cryoshielding device and a twin-blade anti-contaminator, respectively, which closely sandwich the grid. Holey carbon film grids are used as is, or can be glow-discharged, washed with acetone vapor to enhance hydrophilicity, or replaced by continuous non-perforated carbon film grids.

The concentration of the virus suspension is critical for obtaining a thin film with even specimen distribution after blotting; negative staining analysis is used to determine an appropriate range of particle concentration. Another limiting factor is that of the solutes used during virus purification by ultracentrifugation in

gradients such as glycerol, sucrose and cesium chloride. These chemicals will bubble during observation and must be removed by floating the grid on a drop of distilled water (routine for preparing negatively stained samples) or dialysis of the selected virus fractions.

The cryo-negative staining method preserves biological samples in the frozen hydrated state, incorporating negative staining to improve the signal-to-noise ratio of the images. As a contrast agent, ammonium molybdate is normally used (at physiological pH) when this procedure is used for conventional cryo-EM; uranyl formate or acetate is used in the carbon-sandwich method, in which the sample is trapped between two carbon films and is frozen in liquid nitrogen. Unlike air-dried negative staining at room temperature, in the carbon-sandwich method, sample hydration is maintained in all steps (preserving its structural integrity) and specimens are observed at liquid nitrogen temperature [19].

3.3.2 Magnification, Calibration and Minimal Electron Dose

The definition of absolute magnification is necessary, and real magnifications should be calibrated periodically to avoid uncertainty in image processing. The hysteresis of magnetic lenses and changes in specimen height in the objective lens cause small changes in nominal magnification that must be considered in high-resolution studies. Comparisons of three-dimensional reconstruction (3DR) of a virus whose dimensions have been calculated by X-ray analysis is a precise approach to determining the absolute scale; another approach is to mix the test virus with a bacteriophage T4 solution, using the 40.5 Å axial spacing of the bacteriophage tail sheath as an internal magnification standard.

Vitrified specimens are highly sensitive to electron irradiation, and the act of imaging with electrons could eventually destroy the specimen. After insertion of the specimen stage into the microscope, the cryogrid is searched at low magnification ($<$2,000–3,000$\times$) and irradiation levels. An experienced cryomicroscopist is able to select optimal areas by visual inspection; dark areas in the grid are too thick for electron penetration, while bright areas are probably too thin for correct virus particle embedding or can even be dried. Most viruses can be seen directly at low magnification as dark spots, allowing assessment of particle distribution and concentration. These particles are destroyed at high magnification, but can be observed directly for a few seconds as a “bubbling” effect. These sacrificed specimen areas are a convenient form of direct evidence of vitrified specimen quality, assuming that intact adjacent areas in the grid have similar particle concentration and ice thickness.

The strategy for image acquisition is based in this approach, and is done following a relatively “blind” (but not random) procedure, in the sense that the area selected for recording will be seen (and selected or discarded) once the micrograph is developed. Cryo-microscopes are equipped with a low dose system to limit exposure to electrons. The system switches among three states, searching

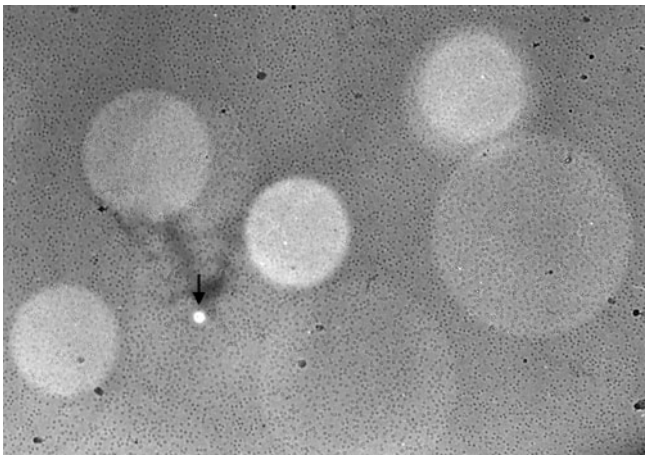

Fig. 3.3 Radiation damage in vitrified bacteriophage T4. In this low magnification field, the smaller circular areas have been sacrificed during focusing; the larger circular areas correspond to recorded regions (the electron dose needed to acquire an image causes no visible effect, but the microscopist exposed the recorded area for longer times to obtain this general view). The bubbling effect can be seen in the particles of some of these exposed areas. The bright area (*arrow*) is literally a hole (made with a focused beam) in the thin vitrified layer that contains the viral particles in suspension

for promising specimen areas at low magnification, focusing at high magnification, and recording at the same high magnification (40,000–60,000×). All of the electrons that pass through the specimen are used to form its image. The image is focused in an adjacent sacrificed area by observing the Fresnel fringes that appear at the edge of radiation-induced bubbles (that first form within the specimen). In this step, astigmatism is corrected and other adjustments are made. Images are recorded with electron doses between 5 $e^-/Å^2$ and 20 $e^-/Å^2$, which produces micrographs of sufficient optical density and signal for subsequent image processing steps (Fig. 3.3).

Imaging on a CCD camera exposes a much smaller sample area, and thus minimizes possible beam-induced specimen movement or charging, similar to the "spot-scan" approach. Inelastic scattering by the sample leads to radiolysis of macromolecules and the embedding medium (vitrified water). The radiolysis products require more space than the original molecules, leading to increase of internal pressure in the sample and ultimately to breakdown (bubbling) of the sample matrix. The pressure increase and the bubbling cause movement in the exposed area of the sample and blurring in the image, thereby attenuating the signal at higher resolution. Inelastic scattering also leads to ejection of electrons from the sample and accumulation of positive charge (sample movement and charging must be minimized).

3.3.3 Imaging Conditions: Contrast Transfer Function

Another drawback in cryo-EM is related to imaging conditions. Images are noisy, because there is no staining agent that enhances the scattering. The amplitude contrast of unstained biological specimens is thus quite low (~10 % or less), and phase contrast is the dominant contrast mechanism, which requires defocusing the microscope objective lens (*i.e.*, images must be deliberately out of focus to enhance contrast). Extensive computer processing is then needed to correct the images and recover structural details.

In a perfect electron microscope, the 2D image recorded on film would be a realistic representation of the projection of the 3D scattering matter in the specimen. As in any other optical system, the image of an object is modulated by the lens characteristics such that each point in the image is the result of a convolution of the corresponding point of the object and a mathematical function, known as the contrast transfer function (CTF). In the case of the electron microscope, the CTF depends on the spherical aberration of the objective lens, the effects of defocusing and inelastic electron scatter, and the partial coherence of the beam. This fundamental concept implies that all TEM images are altered by the CTF and must be corrected for accurate interpretation of the structure of a biological specimen. The CTF is a characteristic function of each microscope (*i.e.*, the spherical aberration coefficient of the objective lens) and the imaging settings (defocus level of the objective lens, beam coherence and accelerating voltage).

By choosing different defocus settings (focal series or pairs are usually taken), specific structural features (or frequencies in the Fourier space) of the image can be accentuated selectively at the expense of others. In appropriate imaging conditions, a contrast-enhancing effect can thus be obtained. CTF-modulated information implies the existence of frequency ranges in which there are no data (zeros in the CTF), regions in which the information has reversed contrast (between the first and the second zero, between the third and fourth zero, and so on), and a fall-off of useful information at higher frequencies (the envelope function), dependent mainly on beam coherence. In the same way that observing a sample by different conventional EM techniques provides complementary data, recording several images at different focal settings to enhance distinct specimen features is a "must-do" (Fig. 3.4).

Cryo-EM micrograph quality can be analyzed by inspection of the CTF zeros or Thon rings in the optical or computed diffraction patterns of images (the sum of the Fourier transform amplitudes is termed the average power spectrum). An image free of aberrations has the signal in the power spectrum as a series of concentric circular rings (zeros or Thon rings) that extends outward from the center of the Fourier transform; the greater the extent of rings, the higher the resolution in the image. Images with drift or astigmatism are easily detected and excluded from further structural analysis (Fig. 3.5).

As good contrast is required for the cryo-micrograph, a compromise should be reached among the factors that modulate contrast. The use of a small objective

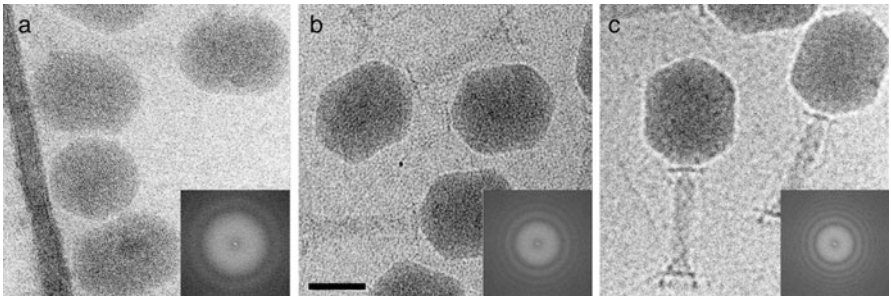

Fig. 3.4 Unstained, frozen, hydrated specimen of phage T4 in vitreous ice, prepared on holey carbon film. Focus series of phage T4 under imaging conditions that enhance dominant spatial frequencies corresponding to (**a**) interstrand spacings between double-stranded DNA filaments (~26 Å) within the head in a relatively close-to-focus image, (**b**) tail sheath spacing (40.5 Å) in a regular defocused image, and (**c**) general morphology in a highly defocused image. Note that detail of the tail is almost lost in the close-to-focus image. Insets show FT (Fourier transform) for each cryomicrograph; the further from focus, the closer the Thon ring is to the FT center. Bar, 50 nm

aperture increases image contrast, but might introduce astigmatism, and lower acceleration voltages increase image contrast, but cause more radiation damage to the specimen. Higher defocus means greater contrast, but also more rapid dampening of the envelope function and many zero transitions of the CTF; CTF of the envelope function is reduced using a brighter beam, such as that generated by FEG. Image contrast can also be improved by additional instrumentation. Energy filters remove inelastically scattered electrons, responsible for much of the noise in micrographs, thus improving the signal-to-noise ratio of the images.

3.4 Cryo-EM Image Processing and Three-Dimensional Reconstruction

Electron microscopes have a large depth of focus compared to virus size. This means that all characteristics at different heights in the virus are in focus simultaneously, and each image recorded in cryo-EM conditions is a 2D projection of 3D scattering density in the specimen. Superposition of all structural information from different levels results in a garbled image. In a single projected view, a specific feature can be derived from any level in the specimen. To reconstruct the native 3D structure, many images must be recorded to obtain different views of the object; viruses tend to be randomly oriented in the vitreous specimen layer [20]. Alternative views can be obtained by tilting the specimen in the microscope. A 10° tilt, which can be accommodated by the anticontaminator, is usually sufficient to give an adequate sampling of orientations. This approach is necessary, for example, to identify the absolute handedness of icosahedral viruses using cryo-EM (see Chap. 2).

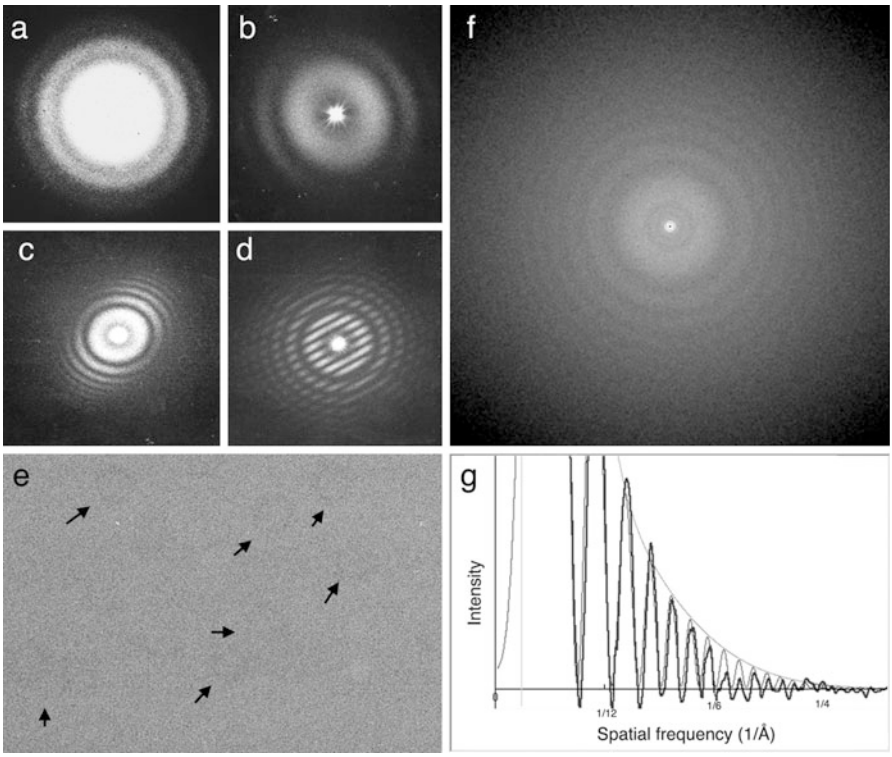

Fig. 3.5 Power spectrum (equivalent to diffraction pattern) analysis of cryomicrographs with distinct aberrations. (**a**) An aberration-free image shows circular concentric Thon rings (zeros). The exact underfocus can be calculated from the first zero position. Signal near the center of the FT corresponds to lower spatial frequencies (low resolution details); signal extending outward from the center corresponds to high spatial frequencies. The last Thon ring indicates the maximum detectable frequency (*i.e.*, resolution) that could be rescued from the 2D projection image. (**b**) Astigmatic migrographs are detected because Thon rings appear elliptical. This aberration can originate from the illumination source and is corrected by the objective lens (an objective aperture that is not well centered can also cause astigmatism). (**c**) Sample drift occurs when resolution is lost preferentially in one direction of the power spectrum. Drift can be thermal (temperature instability in the refrigeration system of the objective lens) or mechanical (stage movement during exposure). Vibrations (acoustic or physical due to liquid nitrogen bubbling in the cryo-stage dewar) limit resolution in all directions. (**d**) Double exposure to determine drift speed. Taking two exposures on the same micrograph, spaced 15–30 s apart, produces a pattern with these typical bands; narrow bands mean larger drift movements and vice versa. (**e**) An excellent image of a rabbit hemorrhagic disease virus solution taken in a FEG 200 kV microscope, in which contrast is very low (*arrows* indicate some viral particles). There is no doubt as to the quality of this micrograph, since the average (**f**) FT calculated from many boxed particle images shows Thon rings to ~4 Å resolution. (**g**) Average power spectrum curve (*thick line*) is used to fit theoretical contrast transfer function (CTF) curves (*thin line*). Underfocus values of 1 μm; first zero of the contrast transfer function at 16 Å

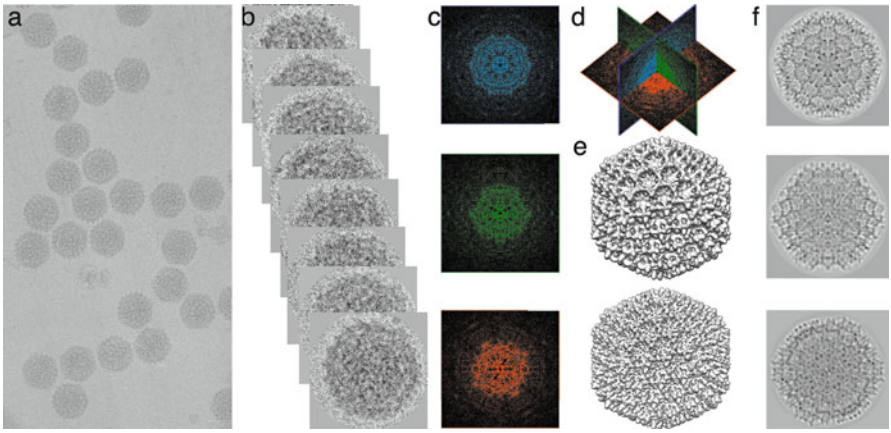

Fig. 3.6 The central section theorem. (**a**) A digitized micrograph containing unstained vitrified viral particles of infectious bursal disease virus (IBDV, a double-stranded RNA virus that infects birds, with a diameter of 650–700 Å). (**b**) Particles are individually selected (*boxed*); (**c**) their 2D FT are calculated from the 2D projections representing different views of the same icosahedral structure. Particle orientation is determined (for example, within 1°) following the projection matching or common lines methods, and the 2D FT are combined in the correct orientation in (**d**) the 3D FT of the virus. (**e**) Accuracy of the initial low resolution 3D map is improved (refined) as the model incorporates more particles and orientation parameters are defined at higher precision in the asymmetric unit. (**f**) Three reprojections from the 3D map are shown

In 1968, DeRosier and Klug found that a 3DR could be recovered from micrographs with 2D images [21], using a mathematical device termed the Fourier transform (FT). Sir Aaron Klug received the Nobel Prize in chemistry in 1982. The FT separates different components of the image into all 2D spatial frequency components (or constituent waves). The FT of each image corresponds to a central plane of the 3D FT of the object density; this is the central section theorem. Distinct projected views fill in different central sections of the transform; the larger the number of views included in the 3D FT, the better the sampling and the 3D object density recovered in Fourier synthesis (Fig. 3.6); many computer programs are available for Fourier analysis and synthesis. In addition to this approach, FT are used for general quality control (evaluating the CTF of each micrograph), correcting the defocus effects (in high resolution studies), and determining particle orientation.

The FT of an image (termed reciprocal or frequency space) is an equivalent, reversible representation of the image (real or Cartesian space). FT provides a mathematical description of the diffraction pattern when imaging an object with a lens (optical or electromagnetic). In the diffraction pattern (the object's FT) produced in the back focal plane of the lens, waves are recombined (positive and negative interference) to form an image. This concept of FT to give a diffraction pattern, followed by Fourier synthesis to produce an image, is central to image processing. In the real-space representation, the parameters that define an image are Cartesian coordinates (x, y, z) and an associated density value. In the FT

representation, these parameters are reciprocal coordinates, an associated amplitude (strength) and an associated phase (which specifies position relative to origin of the wave representing spatial frequency). FT also allows filtering according to spatial frequency. The highest spatial frequencies usually have a large fraction of noise; by eliminating these frequencies in Fourier space and using the inverse FT to convert back to real space, the resulting image is less noisy [22]. The same principles used for 3D image reconstruction are applied for structure determination in X-ray crystallography (Chap. 4).

3.4.1 Digitization

The micrograph must first be scanned with a high precision film scanner to convert it to an array of numbers that represent the darkness on the film; it is then in a form suitable for computer processing. The Shannon sampling theorem states that scanning step size to scan a micrograph should be at least twice as fine as the finest detail to be analyzed (highest frequency or resolution desired), termed the Nyquist sampling. That is, if the resolution desired is 10 Å, 1 pixel should correspond to 5 Å; a 50,000× micrograph scanned with a 7 μm step size corresponds to 1.4 Å/pixel in the specimen; in practice, an image is typically scanned at a scan size of one-fifth to one-third the desired resolution. Another factor to be considered is the limited dynamic range of the cryo-electron micrographs; the scanner should be adjusted to capture this range optimally without image degradation and loss of resolution. This step is omitted if the cryo-electron microscope is equipped with a CCD and digital images are available directly. CCD cameras offer other advantages, such as easy handling, high signal linearity as a function of the number of incoming electrons, and a large dynamic range.

3.4.2 Image Screening

Image quality can be assessed visually by an experienced microscopist to exclude micrographs or CCD frames with high ice contamination, astigmatism, and beam-induced specimen movement. Quantitative analysis is performed by inspection of the CTF rings by calculating the average power spectrum of the micrograph (Fig. 3.4). The CTF is determined by fitting simulated CTF to the observed Thon rings in the calculated power spectrum of the image, which is generally easier for highly defocused images. A CCD camera provides instant feedback for image quality, as FT is calculated dynamically during image acquisition. Once the best micrographs are selected, particles are individually picked (boxed) by manual or automatic methods.

3.4.3 Determination and Refinement of Particle Orientation and Origin

After selection of many thousands of single-particle images (in the best cases), the center of symmetry of each image is established using cross-correlation with a reference image or with the same image rotated 180°. To calculate the 3DR of the object, it must then be determined whether a projection is the front, side or top view, or somewhere in between. Particle orientation determination then begins, that is, the viewing direction relative to the icosahedral symmetry axes. Particle orientations are specified relative to the smallest repeating unit of the icosahedron, termed the asymmetric unit.

The first step of this process requires an initial 3D model as a reference. Many icosahedral virus density maps are available from the Electron Microscopy Data Bank (EMDB: http://www.ebi.ac.uk/pdbe/emdb). The map must be scaled to match the dataset under study, and then low-pass filtered (~35-40 Å resolution) to reduce model bias. A more sophisticated approach involves computing the common lines of a small number of virus images, from which an initial model can be calculated. Due to the inherent difficulties of processing low contrast close-to-focus images, it is often useful to collect focal series with a range of defocus values to facilitate orientation determination. The most time-consuming step when calculating a 3D virus map is the refinement (improvement) of the orientation and center parameters. This analysis involves comparing the particle images with 2D reprojections from a 3D model; projection matching and common lines are the methods most commonly used to determine these parameters [23].

In the projection matching method, the model is projected computationally in all possible directions to generate a set of reference images that are used to match each image with one projection corresponding to the appropriate orientation. The initial low resolution model is updated at the end of each refinement cycle during this iterative process until no further improvement is obtained. Projection matching can be carried out in real or Fourier space.

In the common line method, the central section theorem provides the mathematical foundation for orientation determination of projection images from the same object. The FT of two projection images with different orientations are planes in the 3D FT of the object (a virus) that intersect one another. This intersection line is termed common line and has the same values in each plane for amplitudes and phases (Fig. 3.6).

For an icosahedral virus, a single image with a defined orientation in the asymmetric unit has associated 59 symmetry-related orientations. Each of the 60 equivalent orientations defines the corresponding planes in the 3D FT. The intersection line between any of these planes is known as a self-common line, and there are a maximum of 37 pairs of self-common lines in the FT of a 2D projection image. To estimate individual particle orientation parameters, an exhaustive

search is made for all possible orientations within the asymmetric unit. This method does not require an initial model, but the useful information is limited to the self-common lines.

Cross-common lines arise from the application of icosahedral symmetry between a particle and another particle (with different orientations); there are 60 pairs of cross-common lines between any two images. The orientation angles are initially estimated by assuming an orientation and comparing the agreement of the phases between the common line pairs. All the information in the 2D FT is therefore useful for estimating particle orientation.

3.4.4 Three-Dimensional Reconstruction in Fourier Space and CTF Correction

Considering the central section theorem, and using direct Fourier inversion, a 3D map can be calculated from 2D images [24]. In this method, CTF correction must be applied to the individual particle images before constructing the 3D FT from each 2D FT. It is essential to ensure that sufficient particle orientations have been provided for adequate sampling of Fourier space, since interpolation errors can limit the resolution. This step normally requires intensive memory and computational resources. Although there are other methods for 3D reconstruction of icosahedral viruses, they lie outside our scope here.

The CTF that enables visualization of unstained specimens must be corrected (deconvoluted) to retrieve the high-resolution signal and obtain a 3DR that reliably represents the structure of the specimen. The CTF reverses, removes and attenuates data in frequency ranges in the FT of the image. Precise determination of the Thon ring pattern (CTF zeros or points of minimum contrast) in the power spectrum allows reversing the phases in the appropriate regions of the FT. Multiple images with complementary defocus must be used to fill in the missing data near the zeros. This method is reliable when FEG of high-voltage (200–300 kV) data are used.

3.4.5 Resolution

The resolution of the 3D map depends on the total number of particles, distribution of views within the asymmetric unit, accuracy of center and orientation parameters, the quality of the data (*i.e.*, the radius to which reliable data extend in the FT), and many other factors such as the CTF correction. The resolution in 3DR is less objectively determined than in X-ray crystallography, for which resolution

has come to mean the highest spatial frequency contributing meaningfully to the map [25].

Assessment of the resolution is performed statistically, by splitting the particle set in half and computing two independent maps from each half-set. The two maps (often referred to as even and odd maps) are then correlated as a function of spatial frequency to determine the extent to which the fine structural details have been determined reliably (termed FSC method, Fourier Shell Correlation).

Amplitude scaling is used to restore high-resolution features, using X-ray solution scattering profiles as a reference, or by determining an effective temperature factor (B-factor) (see below). This process of map sharpening scales specific spatial frequencies (resolutions) above others.

Although image variability is a limiting resolution factor, it can also indicate multiple conformations. Conformational states of a macromolecular complex are difficult to classify, as variability must be differentiated from viewing geometry. If these (normally evasive) conformations are assigned to a time-ordered sequence, the resulting density maps can be used to make elegant time-resolved movies of dynamic processes such as virus particle maturation (Chap. 13). As noted above, cryo-EM is the best approach for trapping and visualizing transient structures with a lifetime of a millisecond or longer, as the specimen is rapidly vitrified. Buffer conditions can also be adjusted to extend the lifetime of a transient state; this approach has been used in virus maturation analysis for systems such as herpes simplex virus and several dsDNA bacteriophages (reviewed in [26], an references therein) (see Chap. 13).

3.4.6 Visualization and Structure Representation

Surface rendering of large volume data is very demanding computationally, and can be a rate-limiting step in structural interpretation. For this reason, structural units from the macromolecular complex are normally segmented. Segmentation of individual components permits non-icosahedral averaging of structurally similar components, to enhance signal-to-noise ratio and further improve the resolution of the averaged subunits. For example, the T = 13 capsid of rotavirus allows the nonicosahedral averaging of 13 subunits of VP6 molecules of the asymmetric unit.

In some cases, the structural asymmetric unit boundaries can be established by contouring the map at different levels, based on its compactness and contacts with neighboring densities; homologous models and/or biochemical evidence are generally used. At subnanometer resolutions in the 6–9 Å range, secondary structure elements (SSE) are discernible. The α-helices appear as cylinders of density with diameters of 5–6 Å, and β-sheets as flat densities or planks. An example at this resolution of the final structural model of a spherical virus, the 40 nm-diameter fungal virus *Penicillium chrysogenum* virus (PcV), is shown in Fig. 3.7.

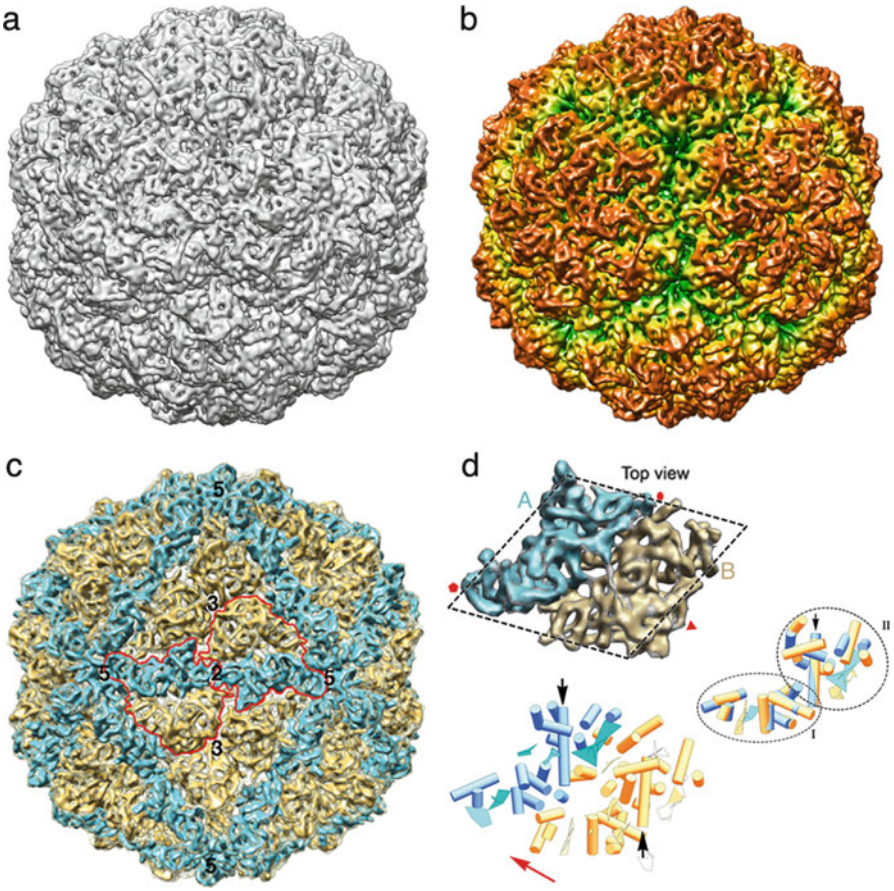

Fig. 3.7 Three-dimensional cryo-EM of the fungal virus Penicillium chrysogenum virus (PcV) at 8.0 Å resolution (based on a FSC threshold of 0.5). (**a**) Surface-shaded representation of the outer surface of the PcV T = 1 (diameter is 400 Å), viewed along a two-fold axis of icosahedral symmetry. Bar, 100 Å. (**b**) As in (a), with the radially color-coded outer surface, which emphasizes the most prominent features as 12 outward-protruding pentamers. (**c**) As in (a); here the asymmetric unit is *cyan* and *yellow*. The asymmetric unit is formed by two ellipsoid-like structures with roughly similar morphology. Boundaries for two asymmetric units are outlined in *red*. Icosahedral symmetry axes are numbered. (**d**) Segmentation of the asymmetric unit, the PcV capsid protein monomer. The *dashed line* highlights the rhomboidal shape, and protein halves A (*cyan*) and B (*yellow*) are indicated (*top left*). At this resolution, secondary structural elements (SSE) of the PcV capsid protein are identified. Cylinders, α-helices; planks, β-sheets. *Black arrows* indicate the ~37 Å-long α-helices of both PcV capsid protein halves. When one of the halves (treated as a rigid body) is superimposed on the other by an ~45-Å translation (*red arrow* indicates translation direction), the relative spatial locations of 13 α-helices and two planar regions are close and require only minor local adjustment. Preserved SSE between both PcV capsid protein halves consist of two domains, domains I and II. This subnanometer resolution analysis indicates that the two PcV capsid protein halves have a comparable structural signature, suggesting ancestral gene duplication (Reproduced/adapted with permission from American Society for Microbiology, ([27], doi:10.1128/JVI.00432-10))

3.4.7 *Hybrid Methods: Combining High-Resolution Structures with Cryo-EM Maps*

As for most research areas, hybrid approaches in structural virology involve multi-disciplinary studies that include a broad set of techniques [28, 29] (see Chap. 7). Here we will refer briefly to the hybridization of atomic structures obtained by X-ray crystallography (see Chap. 4) and by NMR (see Chap. 5) in conjunction with cryo-EM 3DR [30–32]. A more extensive description of combined approaches is included in Chap. 7.

Cryo-EM structural models yield significant information about macromolecular complexes such as viruses (at low to medium resolution), or the folding of individual components (at subnanometer resolution). If more detail is required in the structural model, and higher resolution structural models of individual subunits in the complex are available, the high-resolution structures can be fit ("docked") to the cryo-EM electron density map to obtain a "pseudo-atomic" model of the complex. Fitting tools use rotational and translational searches of a given model within the density map as described in Chap. 7. Such fitting can reveal, for example, interaction interfaces between individual components in atomic detail, providing structural insight into how individual intersubunit interactions might affect complex function. This crucial information cannot, in general, be inferred from the structures of the individual components, and 3D crystals of large functional complexes tend to be very difficult to obtain.

Many studies of large viruses or of the dynamic character of particles that constitute intermediates of virus assembly and function, which are difficult to crystallize, have followed this hybrid approach. Another example is the study of neutralizing monoclonal antibodies and their antigen-binding (Fab) fragments or cell receptors bound to the surface of a virus (see Chaps. 7 and 15). To map the Fab or cell receptor footprint on the virus surface, the antibody-virus complex is studied by cryo-EM and combined with the crystallographic structure of both; this approach was used successfully, for example, for different picornaviruses (rhinovirus, poliovirus and foot-and-mouth disease virus). It is nonetheless possible that the structure of a component will differ when assembled with other components. There are numerous algorithms available for rigid body as well as flexible fitting of components into the larger structure. A quantitative measure of fit accuracy is determined by global and local cross-correlation coefficients.

As the resolution of the cryo-EM map improves, discrepancies in some parts of the individual subunits are evident once fitted into the cryo-EM map; they can be adjusted optimally by permitting flexible fitting of specific domains and/or SSE. Structures in crystals might not always represent conformations related to in situ molecular interactions in physiological conditions. This technique has also been used to validate homology-derived models [33]. Flexible docking can be achieved manually using molecular graphics, but the most-used methods are based on molecular dynamic simulations or on normal mode analysis (Fig. 3.8) (see Chap. 19 for a general description of these theoretical approaches).

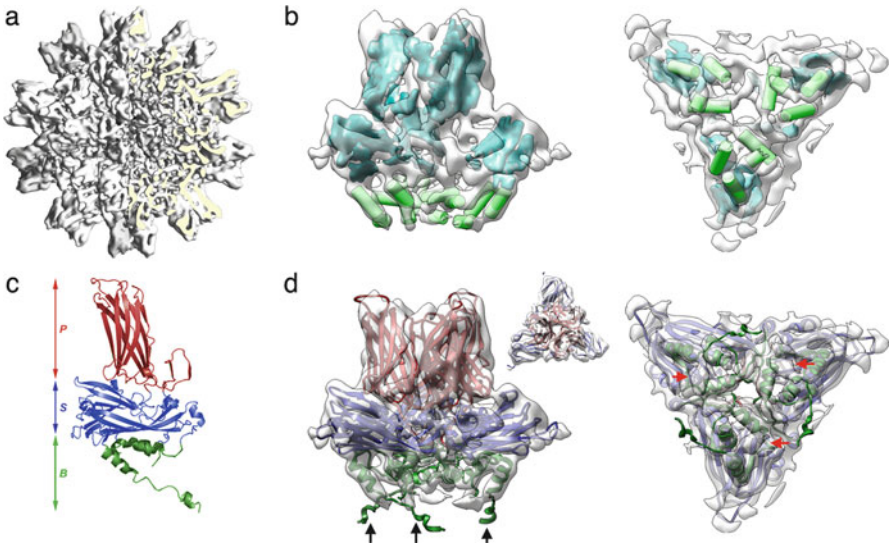

Fig. 3.8 Three-dimensional cryo-EM of T = 1 subviral particles (SVP, ~23 nm in diameter) of IBDV at 7.2-Å resolution. (**a**) Surface-shaded representation of the complete SVP (a quarter has been computationally removed). The most prominent features are 20 VP2 trimeric protrusions of the capsid protein. (**b**) Identification of SSE: green cylinders, α-helices; blue planks, β-sheets. (**c**) The 2.6-Å VP2 X-ray model (PDB entry 2GSY). The VP2 subunit is folded into three domains, termed the projection (*P*), shell (*S*), and base (*B*) domains. Domains S and P are β-barrels. The B domain consists of four N- and C-terminal α-helices that line the inner capsid surface. (**d**) The VP2 trimer X-ray fitted into the corresponding density in the cryo-EM map. The concordance of the two maps is clear in the matching of P and S domain β-barrels. *Arrows* indicate the cut directions to show P and S domain fits (*inset*). Whereas three α-helices fit remarkably well in the cryo-EM structure, a C-terminal α-helix has no corresponding density in the cryo-EM map (*black arrows*), which shows a discernible vacant rod-shaped density adjacent to the C-terminal α-helix (*red arrows*). The proposed movement involves allowed rigid body rotations of the C-α angles in the loop preceding this α-helix. The conformational flexibility of this C-terminal α-helix is critical for IBDV capsid assembly (Reproduced/adapted with permission from American Society for Microbiology ([34], doi:10.1128/JVI.00077-07])

Cryo-EM can also be used as an aid for the atomic resolution of viruses and other biomolecular complexes by X-ray crystallography. Diffraction of crystals of large complexes (such as viruses) requires various phasing methods (see Chap. 4). EM maps are used to solve the phase problem when no phasing by molecular replacement or anomalous scattering is feasible, and heavy atom derivatives do not scatter sufficiently to alter structural factors. A phase extension approach based on molecular envelopes obtained by 3D cryo-EM (or even by conventional negative staining EM) can be used for these crystals (see also Chaps. 4 and 7). If the number of complexes and their positions in the unit cell are known, the envelope specifies those portions of the unit cell whose density is at a constant level. This provides a "solvent flattening" constraint, which with the additional constraint of noncrystallographic symmetry, is imposed iteratively, starting with a low EM resolution

model; the model is progressively improved by introducing diffraction data to higher and higher resolution. This approach has worked well with a number of icosahedral viruses.

3.5 Near-Atomic Resolution of Virus Structures by Cryo-EM

High-resolution 3D cryo-EM is becoming an important structural tool for determining detailed 3D structures of large biological complexes, such as viruses, that are often too large or too heterogeneous to be studied by "conventional" high-resolution methods like X-ray crystallography (Chap. 4) and NMR spectroscopy (Chap. 5) [25, 35–37]. Several recent studies with icosahedral viruses have pushed the limit of single-particle cryo-EM reconstruction to near-atomic resolution (~3.6–4.5 Å). At this resolution, many detailed structural features can be resolved, including deep grooves and pitches of helices, interstrand distance of ~4.4 Å in β-sheets (except for hydrogen-bonded regions), densities for loops and voluminous amino acid side chains, and the zigzag pattern of Cα atoms separated by ~3.8 Å [38]. These structural data can be used as constraints to trace amino acid backbones (Cα model building) using modeling tools. When the X-ray model is available, comparison of the X-ray and cryo-EM structures of the same virus reveals excellent agreement to the level of amino acid side chains.

Several factors have contributed synergistically to this improvement in resolution:

1. *Sample handling*. Structural homogeneity is more important than purity. It is desirable to avoid possible structural damage caused by density gradient centrifugation, since structural heterogeneity (disorder) can be a limiting factor. Icosahedral viruses are regular, more rigid structures than lipid-containing viruses. Dynamics states (*i.e.*, conformational flexibility) also limit resolution.
2. *Cryo-EM imaging*. Improvements in cryo-EM instrumentation such as more stable electron beams and sample holders have reduced specimen drift, a limiting factor in achieving atomic resolution. The high voltage cryo-microscope (FEG, 300 kV) must be optimally aligned so that the electron beam is parallel, with minimal beam tilt. Only those images with visible CTF rings up to 5 Å in their power spectra should be selected (the resolution of the 3DR usually extends beyond the last detectable of Thon ring).
3. *Computational methods for processing noisy cryo-EM images*. Structure refinement is carried out as a two-step, iterative procedure based on projection matching, orientation-origin parameter determination and 3DR by gradually pushing toward higher resolution. High-resolution images are often recorded under close-to-focus conditions, and many thousands of these low-dose phase-contrast images must be used to enhance the high-resolution features. This enormous number of particle images is also related to the fall-off in the Fourier amplitudes at high spatial frequencies (equivalent to high B factor in X-ray

crystallography). Resolution is evaluated by the FSC criterion or by directly evaluating the structural features resolved in the reconstructed map. As in X-ray structures, some regions can have lower resolution than others, probably due to local intrinsic flexibility.

4. *Atomic modeling tools optimized for use with cryo-EM-derived density maps*. Map quality of some protein subunits can be improved by averaging quasi-equivalent subunits, *i.e*., viral capsids with a triangulation (T) number higher than 1 (provided that these subunits are found in similar conformations) (see Chap. 2). An empirical B factor can be estimated by a trial-and-error method that evaluates features such as continuity of backbone and side-chain densities; this can improve high-resolution features and prevent over-sharpening. At this resolution, individual structural components are segmented from the entire capsid and used for model building. At near-atomic resolution (~4 Å), backbone tracing is difficult and error-prone, as some densities are branched and side-chains are limited. Homologous structures obtained by sequence-based comparative modeling can also be used. There are modeling methods adapted to the characteristics of cryo-EM density maps, and modeling tools used in protein crystallography can be adjusted to verify models derived from cryo-EM maps. Evaluation of the atomic models follows the same restrictions used in X-ray crystallography (consistency with protein sequence and reasonable Ramachandran plot, among others). In any case, uncertainties are unavoidable in interpreting maps at 3.5–4.5 Å. Resolved cryo-EM maps are thus a combination of full-atom residue models (SSE-rich regions) and Cα models (regions with less-defined densities).

Near-atomic resolution of virus structures that address important biological questions has been reported for a still-limited number of viruses (reviewed in [24, 25, 35], and references therein). Cytoplasmic polyhedrosis virus was the first example (at 3.88 Å resolution) of a complete *de novo* chain trace from cryo-EM maps. Other examples include the double- and triple-layered rotaviruses, which were unambiguously equivalent to the X-ray model (Fig. 3.9); dsDNA bacteriophage ε15, which is related to bacteriophage HK97; P22, which was resolved in two morphogenetic states; bovine papillomavirus (at 3.6 Å resolution), a dsDNA eukaryotic in which key interactions were described in particle assembly; human adenovirus, which shows how the cement proteins tie together the map structural proteins in the icosahedral capsid; and dsRNA aquareovirus (at 3.3 Å resolution), which showed a priming mechanism for cell entry.

3.6 Reconstructing Viruses Without Imposing Symmetry

Many icosahedral symmetry-based virions present features/structures that do not obey icosahedral symmetry. Examples include the packaging complex, the tail or the core in the capsid interior of dsDNA tailed bacteriophages [40]. These

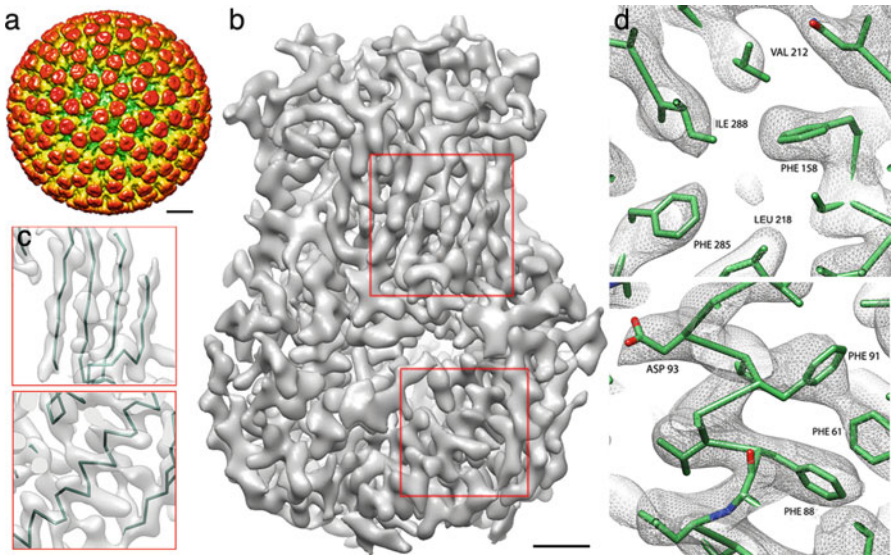

Fig. 3.9 High resolution rotavirus VP6 structure generated by 3D single-particle cryo-EM. A total of 18,125 images of rotavirus double-layered particles (DLP) collected at 300 kV were downloaded from the Grigorieff lab web page at Brandeis University (http://emlab.rose2.brandeis.edu/), and processed using Xmipp software. (**a**) Rotavirus DLP-filtered at ~25 Å. Bar, 100 Å. (**b**) VP6 trimer after 13-fold averaging at ~4 Å resolution. At this resolution, α-helices, β-sheets and densities for loops and bulky amino acid side chains are seen. Bar, 10 Å. (**c**) Close-up of selected VP6 regions included in the squares in (**b**) with the corresponding X-ray structure (PDB 1QHD). Individual β-strands (*top*) and deep grooves and pitches of α-helices (*bottom*) are seen clearly. (**d**) Densities in selected VP6 areas, shown with the atomic model of VP6; bulky side-chain densities match the X-ray structure. These structures are similar to those published by Grigorieff's group [39]

non-icosahedral components can have their own symmetry, which is obscured by the symmetry mismatch with the icosahedral capsid shell (see Chaps. 12 and 17). A map without icosahedral symmetry requires at least 60 times as much data to achieve a similar resolution. Elaborate approaches during the data processing step have enabled structural resolution of complex viruses as a single entity without imposing symmetry, using projection-matching techniques to orient the particles. The asymmetric orientation of a particle is initially determined by a time-consuming search of all possible orientations.

In the case of the T4 phage, the capsid and the tail were reconstructed separately by cryo-EM, after which the atomic models of their component proteins were fitted to determine how the individual parts contribute to the function of this complex molecular machine [41, 42] (see Chap. 11).

3.7 Reconstructing Viruses with Helical Symmetry

The capsids of many plant viruses and bacteriophages have helical symmetry [43]. In addition, the genome of some enveloped animal viruses is surrounded by a helical symmetry-based nucleocapsid; these include filoviruses (Ebola and Marburg viruses), rhabdoviruses (rabies and vesicular stomatitis viruses (VSV)), paramyxoviruses (measles and mumps), orthomyxoviruses (influenza virus) and retroviruses (human immunodeficiency virus, HIV) (see Chap. 2). In certain non-physiological conditions, some capsid proteins of icosahedral viruses may assemble into helical structures, revealing an intrinsic structural polymorphism. Helical viruses and capsids do not crystallize, and many such structures have been determined using X-ray fiber diffraction methods at high resolution. Cryo-EM recently supplied structures at ~10 Å resolution for the VSV virion trunk [44] and 3.3 Å for tobacco mosaic virus (TMV) [45], which allowed the construction of a *de novo* atomic model of TMV in a state that is biologically relevant to its assembly/disassembly.

The redundancy intrinsic to helical assemblies renders them optimal for cryo-EM averaging, since a single image provides all the projection images needed to reconstruct the 3D structure. Helical parameters are determined by measuring the pitch of the helix from layer lines in the FT of the tubular structure. A 2D classification is usually made if structural variability or heterogeneity is detected (or suspected). The 3DR is computed using the iterative helical real space reconstruction (IHRSR) method, a single-particle type approach that does not require long high-ordered filaments. The IHRSR algorithm uses the helical symmetry as a constraint to impose it on asymmetric reconstructions [46].

3.8 Cryo-Electron Tomography of Viruses

3.8.1 Basic Concepts and General Experimental Design

A preparation of icosahedral viruses observed by cryo-EM normally provides multiple views with random orientations of identical particles (without considering structural heterogeneity). Many enveloped viruses are pleomorphic, however; examples include orthomixo-, paramyxo-, retro- and poxviruses (see Chap. 11). Herpesviruses and other enveloped viruses are intermediate forms, with an icosahedral capsid surrounded by a pleomorphic structure made of protein and lipid layers (see Chap. 2). The structural variability of all these viruses means that each particle has a different shape, size or conformation, and 3DR by averaging cryo-EM images as described above is not possible. However, a reconstructed 3D image can be produced by obtaining multiple views of a single viral particle. To do this, the

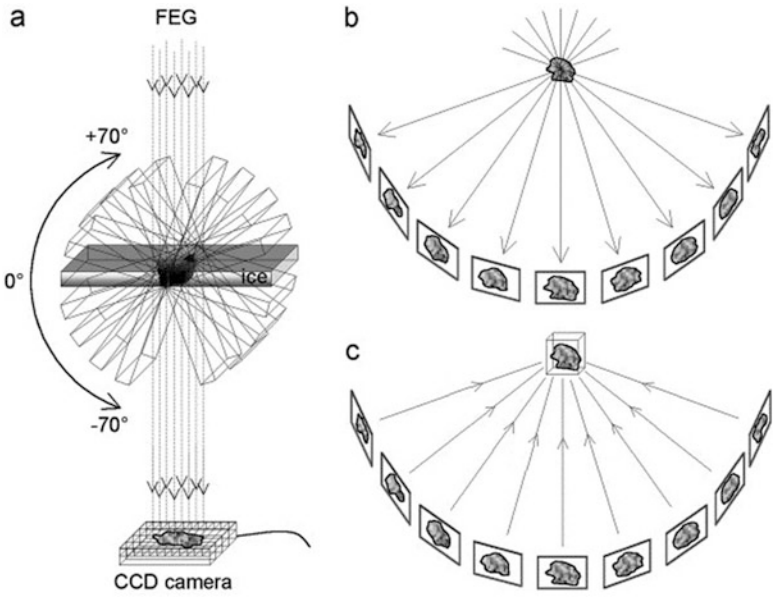

Fig. 3.10 Electron tomography. (**a**) 2D projection images are acquired on a CCD camera while the same specimen area embedded in a vitreous thin layer is tilted incrementally (~1–2°, tilt range ± 70°). (**b**) Diagram illustrating the images projected by a specimen at successive tilt angles. (**c**) After mutual alignment of all these 2D projection images, a density map (tomogram) is reconstructed by a weighted backprojection procedure (Adapted from [47]. Courtesy of W. Baumeister)

specimen is tilted around an axis perpendicular to the electron beam inside the microscope. This type of cryo-EM is termed cryo-ET. Tilting of the specimen provides images of the same field of view (typically more than 100), for example, over a range of ±70° at steps of 1° or 2° (limited by the design of specimen holders and because specimen thickness increases very rapidly at high tilt angles) (Fig. 3.10).

The 3D structure, or tomogram, is calculated as a back-projection in real space; assembly of correctly aligned projections is reverse-projected into 3D space. Cryo-ET has allowed the study of viruses not only in their native physiological state, but also in their natural cell environment (see Chap. 14), thereby providing a bridge between structural studies at the molecular and cellular levels (reviewed in [23, 48, 49], and references therein).

To obtain a detailed, undistorted reconstruction, the tilt series must cover as wide an angular range as possible in as many increments as possible. Tomogram resolution is limited because the range of angles sampled is incomplete and there are no data in some parts of the 3D FT (the missing wedge); in addition, data are missing in the spaces between sampled planes. At the same time, the electron dose must be

kept as low as possible to avoid radiation damage. In principle, a total dose (~100 $e^-/Å^2$) is fractioned over the entire tilt series (~1 $e^-/Å^2$ per image), but the resulting projections are very noisy, making their alignment and CTF correction unreliable. This dose represents less than 5 % of the exposure normally used for single-particle cryo-EM. To increase contrast, images are taken at high defocus values (at least 3–10 μm; compared to 0.5–3 μm for cryo-EM), and resolution is somewhat lower than the first zero of the CTF (in the 4 nm range), as restoration of the true projection is difficult with these low signal-to-noise ratio micrographs. These limitations can be overcome with a double-tilt series; two single-tilt series of the objects are recorded, during which the specimen is rotated by 90° around the beam direction after the first series. The resolution problem is also reduced, if applicable, by image averaging of selected regions (homogeneous subcomponents such as glycoproteins or capsids) of the polymorphic (heterogeneous) viruses.

A cryo-ET setup consists of a high voltage cryo-electron microscope equipped with a FEG, a CCD camera and possibly an energy filter. Automation of the acquisition process is essential for acquiring tomographic data sets in low-dose conditions. High voltage electrons can penetrate thicker samples, which enables imaging of cells or organelles. The interaction of electrons with thick (>200 nm) specimens produces many inelastic scattering events, leading to strong blurring. Energy filters allow imaging of thick specimens and are indispensable for tomography of whole ice-embedded cells or other objects of 0.5–1 μm thickness. Cryo-sectioning is a solution for very thick specimens frozen at high pressure. Without sectioning, only the peripheral areas of flat cells are accessible to cryo-ET.

3DR of an object from its projections involves two steps; first, the micrographs must be aligned to a common coordinate system, and second, the aligned micrographs are merged into a tomogram. Fiducial markers added to the specimen (typically colloidal gold), which appear as high-density dots in the images, are commonly used for alignment, although this can also be done without markers. The most common reconstruction method in cryo-ET is the weighted back-projection, to form a 3DR. Because of uneven sampling in the Fourier space, the low frequencies are artificially enhanced, which requires weighting of projections prior to back-projection to obtain a reliable reconstruction.

The interpretation of tomograms at the ultrastructural level requires decomposition of a tomogram into its structural components, *e.g.*, the segmentation of defined components such as membranes and glycoproteins. Manual assignment of features is commonly used. In addition, to increase the signal-to-noise ratio, so-called denoising algorithms have been developed for analysis and three-dimensional visualization.

Cryo-ET maps of viral complexes at 20–40 Å resolution can be obtained by 3D averaging of different subtomograms from the same particle. Of course, single-particle cryo-EM provides higher resolution maps with an unbiased starting model. Cryo-ET can provide reliable starting models that are then refined by single-particle analysis. In addition to 3D alignments, processing subvolumes can require classification analysis.

3.8.2 *Structure of Pleomorphic Viruses and Capture of Viral Life Cycles Using Cryo-ET*

Cryo-ET has been applied to the visualization of the 3D structures of non-isometric virus particles (reviewed in [50, 51], and references therein); for example, it has been used to study the architecture of influenza virus, herpesvirus, immunodeficiency viruses and vaccinia virus, among other enveloped viruses (Fig. 3.11a).

Influenza virus has two types of protein spikes emerging from its envelope, hemagglutinin (HA) and neuraminidase (NA); there are about 400 densely-packed spikes (85 % HA, 15 % NA) and NA spikes tend to cluster; in addition, HA molecules show conformational changes after fusion with liposomes. Cryo-ET of intact virions of herpes simplex virus 1 (HSV-1) has provided new information about the pleomorphic structures crucial for infection of host cells: tegument (an amorphous protein layer that includes host structures such as actin filaments) and an envelope coated with glycoprotein spikes. The icosahedral $T = 16$ capsid enclosing the viral DNA adopts an eccentric position within the approximately spherical virus. The capsid images were extracted from tomograms, averaged, and compared to the nontegumented capsid, revealing capsid-tegument contacts. The entry portal (a specialized DNA packaging vertex) in different herpesvirus capsids was also visualized in one of the 12 five-fold vertices. An equivalent cryo-ET study to detect asymmetric components inside icosahedral viruses was performed with poliovirus, a ~30 nm icosahedral virus that lacks an envelope; isolate particles were imaged releasing their genome, and RNA exited through channels near the two-fold axes. Cryo-ET of the vaccinia virus identified a complex shell consisting of different layers, in which the inner core membrane incorporates pore-like formations. Envelope glycoproteins (env, gp120) of simian and human immunodeficiency viruses (SIV and HIV) mediate binding to the receptor CD4 to initiate infection; analysis by cryo-ET showed that env trimers change conformation in order to interact with the cell receptor.

Beyond the study of purified viruses, cryo-ET extends its scope to different stages of the viral life cycle and cell pathogenesis (cell-associated state) [57, 58]. Until recently, this information was derived mainly from EM of thin sections of plastic-embedded virus-infected cells; the specimen is chemically fixed, dehydrated in organic solvents, embedded in a resin or plastic, and sectioned. The slices are stained to increase contrast. For cryo-ET, the slices are usually 200–500 nm thick. This differs from the thin (20–100 nm) sections usually used in serial section reconstruction, in which single images of individual thin sections are merged computationally to obtain a 3DR, limiting the resolution in the z-axis to the slice thickness. Specimen thickness is a limiting factor for the preservation of native ultrastructure (unless the high pressure freezing approach is used). Cryo-ET of cells is restricted to unsectioned thin prokaryotic cells and to peripheral thin regions of eukaryotic cells that are flattened, and thus transparent to the electron beam. Analysis of larger cells requires technically challenging cryosectioning.

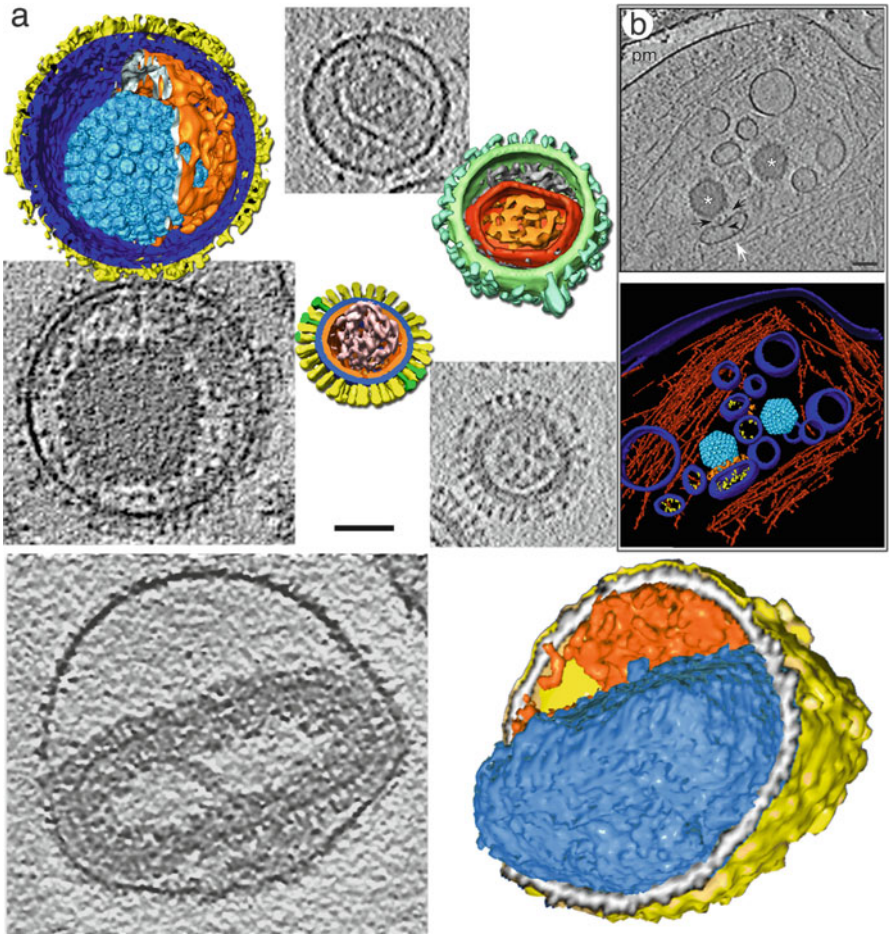

Fig. 3.11 Cryo-ET of pleomorphic viruses and viral life cycles. (**a**) Tomographic reconstructions of HSV-1 (*left*), Rous sarcoma virus (RSV, *right top*), influenza A virus (*right bottom*) and vaccinia virus (VV, *bottom*). Surface-shaded representations of the tomograms are cut to see the virion interior, and a slice of each tomogram is shown. HSV-1 has a T = 16 capsid (*light blue*) buried in the proteinaceous tegument (*orange*), surrounded by a membrane (*dark blue*) studded with glycoprotein spikes (*yellow*) (Adapted from [52]). The RSV virion has a polyhedral capsid (*red*) with an internal density that corresponds to the viral genome (*orange*), surrounded by the matrix protein layer (*grey*); the outermost membrane with the Env spikes is *green* (Adapted from [53]). The genome of influenza A virus is organized as ribonucleoprotein complexes (*pink*); the matrix protein layer (*orange*) is resolved from the lipid bilayer (*blue*); the glycoproteins HA (*yellow*) and NA (*green*) are distinguishable (Adapted from [54]; all three figures courtesy of A.C. Steven). VV mature virion comprises an internal core (*blue*) and the lateral body (*orange*) surrounded by an envelope (Adapted from [55]; courtesy of J.L. Carrascosa). Bar, 50 nm. (**b**) Secondary envelopment of HSV-1 capsids at axon terminals. Slice of the tomogram (*top*) of an intact axon terminal (*asterisks*, capsids; *white arrow*, enveloping vesicle; *arrowhead*, glycoproteins; *black arrows*, tegument; *pm*, plasma membrane). Bar, 100 nm. Surface-shaded representation of the tomogram (*bottom*); color code as in (a); actin is in *red* (Adapted from [56], doi:10.1371/journal.ppat.1002406)

Cryo-ET of the ε15 bacteriophage infecting its bacterial host has allowed visualization of structural changes in the tail machinery, including a tubular density that spans the periplasmic space of the bacterial wall that is the conduit for viral DNA entry into the cell. HSV-1 virions entering synaptosomes (subcellular structures) were caught in action in 3D using cryo-ET; the viral envelope fuses directly with the host membrane, followed by detegumentation. Cryo-ET of frozen-hydrated neurons showed that most egressing capsids were transported independently of the viral envelope; this indicates that progeny herpes viruses are transported along axons as subassemblies and not as complete virions within transport vesicles. Secondary envelopment takes place in axon terminals (Fig. 3.11b). The life cycle of murine gammaherpesvirus, including viral attachment, entry, assembly in virus-induced nuclear inclusion bodies and egress, has been also tracked using cryo-ET. Cryo-ET studies of intact plunge-frozen human cells showed that, during HIV assembly in the native budding sites, the polyprotein Gag lattice is indistinguishable from that of the released immature virion; loss of control of proteolytic maturation led to the formation of aberrant particles.

3.9 Understanding Viruses: Some Major Contributions of Electron Microscopy and Tomography

The first icosahedral virus reconstructions from EM images were made in 1970 from just six negatively stained TBSV (tomato bushy stunt virus) particles at 28 Å resolution, and two of human papillomaviruses at 60 Å [59]. Based on numerous structural virology studies, outstanding progress has been made in the last 40 years. EM imaging has become an indispensable tool in structural virology, and determination of structure is the key to understanding function.

Single-particle cryo-EM has allowed routine analysis of many viral macromolecular complexes in native environments at subnanometer resolutions, in some instances to near-atomic resolution. Cryo-EM is applicable to capsids, genome packaging motors, bacteriophage tails, and other asymmetric supramolecular assemblies (for example, viral polymerase complexes and filamentous ribonucleoprotein complexes). Cryo-EM is best suited to the study of viral complexes too flexible or too scarce to be crystallized for X-ray diffraction studies, or too large for NMR spectroscopy analysis. The most notable feature of cryo-EM is the ability to determine virus structure in its native environment, which permits structural studies of metastable and transient functional intermediate states. The resolution of multiple states will be central to the discovery of molecular mechanisms. 3DR of icosahedral viruses at near-atomic resolution show that atomic models can be derived from cryo-EM images, yielding valuable new information about virus life cycles.

Cryo-ET allows the study of heterogeneous samples such as pleomorphic viruses, and analysis of virus structures in the cellular context, a frontier in

structural virology. Analysis of virus-cell interactions will contribute to the development of strategies to combat a large variety of human, animal and plant viral diseases.

3.10 Perspectives

Although the molecular targets for X-ray crystallography and cryo-EM have begun to overlap as these techniques have been perfected, the synergy between them is clear (see also Chap. 7). Cryo-EM and cryo-ET will continue to provide insights into the structure of large, flexible, biologically relevant macromolecular viral assemblies in increasing, unprecedented detail. Whereas single-particle cryo-EM is a well-established and popular tool for structure analysis, with some anticipated improvements in instrumentation and software, cryo-ET is expected to evolve rapidly in coming years. Introduction of direct electron detectors instead of CCD will improve signal transfer efficiency in cryo-imaging. Likewise, the phase plate cryo-electron microscope has shown promising results in acquiring high-contrast, close-to-focus images with high-resolution information. The need remains for better computational methods for alignment, classification and CTF correction of low-contrast images.

Acknowledgements I thank Daniel Luque for stimulating discussions, José L. Carrascosa and José M. Valpuesta for continuous support, comments and careful reading of the manuscript, Alasdair C. Steven and Benes L. Trus for advice and encouragement and Catherine Mark for editorial help. I am indebted to current and former members of my group (Irene Saugar, Daniel Luque, Nerea Irigoyen, Elena Pascual, Josué Gómez-Blanco, Mariana Castrillo, Ana Correia and Carlos Pérez) and other colleagues for their hard work, skills and enthusiasm that made work possible and enjoyable. This work was supported by grant BFU2011-25902 from the Spanish Ministry of Science and Innovation.

References and Further Reading

1. Alberts B, Johnson A, Lewis J, Raff M, Roberts K, Walter P (2007) Molecular biology of the cell. Garland Science, New York
2. Nogales E, Grigorieff N (2001) Molecular machines: putting the pieces together. J Cell Biol 152:F1–F10
3. Steven A, Belnap D (2005) Electron microscopy and image processing: an essential tool for structural analysis of macromolecules. Curr Protoc Protein Sci Chapter 17:Unit 17 12
4. Klug A (2010) From virus structure to chromatin: X-ray diffraction to three-dimensional electron microscopy. Annu Rev Biochem 79:1–35
5. Harrison SC (2004) Whither structural biology? Nat Struct Mol Biol 11:12–15
6. Baumeister W, Steven AC (2000) Macromolecular electron microscopy in the era of structural genomics. Trends Biochem Sci 25:624–631
7. Steven AC, Baumeister W (2008) The future is hybrid. J Struct Biol 163:186–195

8. Lasker K, Phillips JL, Russel D, Velazquez-Muriel J, Schneidman-Duhovny D, Tjioe E, Webb B, Schlessinger A, Sali A (2010) Integrative structure modeling of macromolecular assemblies from proteomics data. Mol Cell Proteomics 9:1689–1702
9. Goldsmith CS, Miller SE (2009) Modern uses of electron microscopy for detection of viruses. Clin Microbiol Rev 22:552–563
10. Bozzola JJ, Russell LD (1999) Electron microscopy. Principles and techniques for biologist. Jones and Bartlett Publishers, Boston
11. Dubochet J, Adrian M, Chang JJ, Homo JC, Lepault J, McDowall AW, Schultz P (1988) Cryo-electron microscopy of vitrified specimens. Q Rev Biophys 21:129–228
12. Amos LA, Henderson R, Unwin PN (1982) Three-dimensional structure determination by electron microscopy of two-dimensional crystals. Prog Biophys Mol Biol 39:183–231
13. Henderson R (2004) Realizing the potential of electron cryo-microscopy. Q Rev Biophys 37:3–13
14. Harris JR (1997) Negative staining and cryoelectron microscopy: the thin film techniques. BIOS Scientific Publishers Ltd., Oxford
15. Wild P (2008) Electron microscopy of viruses and virus-cell interactions. Methods Cell Biol 88:497–524
16. Leiman PG, Kanamaru S, Mesyanzhinov VV, Arisaka F, Rossmann MG (2003) Structure and morphogenesis of bacteriophage T4. Cell Mol Life Sci 60:2356–2370
17. Cavalier A, Spehner D, Humbel BM (eds) (2008) Handbook of cryo-preparation methods for electron microscopy. CRC Press, London
18. Baker TS, Olson NH, Fuller SD (1999) Adding the third dimension to virus life cycles: three-dimensional reconstruction of icosahedral viruses from cryo-electron micrographs. Microbiol Mol Biol Rev 63:862–922
19. De Carlo S, Stark H (2010) Cryonegative staining of macromolecular assemblies. Methods Enzymol 481:127–145
20. Crowther RA (2008) The Leeuwenhoek lecture 2006. Microscopy goes cold: frozen viruses reveal their structural secrets. Philos Trans R Soc Lond B Biol Sci 363:2441–2451
21. De Rosier DJ, Klug A (1968) Reconstruction of three dimensional structures from electron micrographs. Nature 217:130–134
22. Moody MF (1990) Image analysis of electron micrographs. In: Hawkes PW, Valdré U (eds) Biophysical electron microscopy. Basis concepts and modern techniques. Academic Press, London, pp 145–288
23. Rochat RH, Chiu W (2012) Cryo-electron microscopy and tomography of virus particles. In: Egelman EH (ed) Comprehensive biophysics, biophysical techniques for structural characterization of macromolecules, vol 1. Academic Press, Oxford, pp 311–340
24. Chang J, Liu X, Rochat RH, Baker ML, Chiu W (2012) Reconstructing virus structures from nanometer to near-atomic resolutions with cryo-electron microscopy and tomography. Adv Exp Med Biol 726:49–90
25. Grigorieff N, Harrison SC (2011) Near-atomic resolution reconstructions of icosahedral viruses from electron cryo-microscopy. Curr Opin Struct Biol 21:265–273
26. Steven AC, Heymann JB, Cheng N, Trus BL, Conway JF (2005) Virus maturation: dynamics and mechanism of a stabilizing structural transition that leads to infectivity. Curr Opin Struct Biol 15:227–236
27. Luque D, Gonzalez JM, Garriga D, Ghabrial SA, Havens WM, Trus B, Verdaguer N, Carrascosa JL, Castón JR (2010) The T=1 capsid protein of penicillium chrysogenum virus is formed by a repeated helix-rich core indicative of gene duplication. J Virol 84:7256–7266
28. Johnson JE (2008) Multi-disciplinary studies of viruses: the role of structure in shaping the questions and answers. J Struct Biol 163:246–253
29. Russel D, Lasker K, Phillips J, Schneidman-Duhovny D, Velazquez-Muriel JA, Sali A (2009) The structural dynamics of macromolecular processes. Curr Opin Cell Biol 21:97–108
30. Tang L, Johnson JE (2002) Structural biology of viruses by the combination of electron cryomicroscopy and X-ray crystallography. Biochemistry 41:11517–11524

31. Topf M, Lasker K, Webb B, Wolfson H, Chiu W, Sali A (2008) Protein structure fitting and refinement guided by cryo-EM density. Structure 16:295–307
32. Rossmann MG, Morais MC, Leiman PG, Zhang W (2005) Combining X-ray crystallography and electron microscopy. Structure 13:355–362
33. Topf M, Sali A (2005) Combining electron microscopy and comparative protein structure modeling. Curr Opin Struct Biol 15:578–585
34. Luque D, Saugar I, Rodriguez JF, Verdaguer N, Garriga D, Martin CS, Velazquez-Muriel JA, Trus BL, Carrascosa JL, Castón JR (2007) Infectious bursal disease virus capsid assembly and maturation by structural rearrangements of a transient molecular switch. J Virol 81:6869–6878
35. Zhou ZH (2011) Atomic resolution cryo electron microscopy of macromolecular complexes. Adv Protein Chem Struct Biol 82:1–35
36. Zhou ZH (2008) Towards atomic resolution structural determination by single-particle cryo-electron microscopy. Curr Opin Struct Biol 18:218–228
37. Hryc CF, Chen DH, Chiu W (2011) Near-atomic-resolution cryo-EM for molecular virology. Curr Opin Virol 1:110–117
38. Yu X, Jin L, Zhou ZH (2008) 3.88 A structure of cytoplasmic polyhedrosis virus by cryo-electron microscopy. Nature 453:415–419
39. Zhang X, Settembre E, Xu C, Dormitzer PR, Bellamy R, Harrison SC, Grigorieff N (2008) Near-atomic resolution using electron cryomicroscopy and single-particle reconstruction. Proc Natl Acad Sci U S A 105:1867–1872
40. Briggs JA, Huiskonen JT, Fernando KV, Gilbert RJ, Scotti P, Butcher SJ, Fuller SD (2005) Classification and three-dimensional reconstruction of unevenly distributed or symmetry mismatched features of icosahedral particles. J Struct Biol 150:332–339
41. Kostyuchenko VA, Chipman PR, Leiman PG, Arisaka F, Mesyanzhinov VV, Rossmann MG (2005) The tail structure of bacteriophage T4 and its mechanism of contraction. Nat Struct Mol Biol 12:810–813
42. Aksyuk AA, Rossmann MG (2011) Bacteriophage assembly. Viruses 3:172–203
43. Stubbs G, Kendall A (2012) Helical viruses. Adv Exp Med Biol 726:631–658
44. Ge P, Tsao J, Schein S, Green TJ, Luo M, Zhou ZH (2010) Cryo-EM model of the bullet-shaped vesicular stomatitis virus. Science 327:689–693
45. Ge P, Zhou ZH (2011) Hydrogen-bonding networks and RNA bases revealed by cryo electron microscopy suggest a triggering mechanism for calcium switches. Proc Natl Acad Sci U S A 108:9637–9642
46. Egelman EH (2007) Single-particle reconstruction from EM images of helical filaments. Curr Opin Struct Biol 17:556–561
47. Grunewald K, Medalia O, Gross A, Steven AC, Baumeister W (2003) Prospects of electron cryotomography to visualize macromolecular complexes inside cellular compartments: implications of crowding. Biophys Chem 100:577–591
48. Lucic V, Forster F, Baumeister W (2005) Structural studies by electron tomography: from cells to molecules. Annu Rev Biochem 74:833–865
49. Cope J, Heumann J, Hoenger A (2011) Cryo-electron tomography for structural characterization of macromolecular complexes. Curr Protoc Protein Sci Chapter 17:Unit17 13
50. Subramaniam S, Bartesaghi A, Liu J, Bennett AE, Sougrat R (2007) Electron tomography of viruses. Curr Opin Struct Biol 17:596–602
51. Grunewald K, Cyrklaff M (2006) Structure of complex viruses and virus-infected cells by electron cryo tomography. Curr Opin Microbiol 9:437–442
52. Grunewald K, Desai P, Winkler DC, Heymann JB, Belnap DM, Baumeister W, Steven AC (2003) Three-dimensional structure of herpes simplex virus from cryo-electron tomography. Science 302:1396–1398
53. Butan C, Winkler DC, Heymann JB, Craven RC, Steven AC (2008) RSV capsid polymorphism correlates with polymerization efficiency and envelope glycoprotein content: implications that nucleation controls morphogenesis. J Mol Biol 376:1168–1181

54. Harris A, Cardone G, Winkler DC, Heymann JB, Brecher M, White JM, Steven AC (2006) Influenza virus pleiomorphy characterized by cryoelectron tomography. Proc Natl Acad Sci U S A 103:19123–19127
55. Cyrklaff M, Risco C, Fernandez JJ, Jimenez MV, Esteban M, Baumeister W, Carrascosa JL (2005) Cryo-electron tomography of vaccinia virus. Proc Natl Acad Sci U S A 102:2772–2777
56. Ibiricu I, Huiskonen JT, Dohner K, Bradke F, Sodeik B, Grunewald K (2011) Cryo electron tomography of herpes simplex virus during axonal transport and secondary envelopment in primary neurons. PLoS Pathog 7:e1002406
57. Fu CY, Johnson JE (2011) Viral life cycles captured in three-dimensions with electron microscopy tomography. Curr Opin Virol 1:125–133
58. Iwasaki K, Omura T (2010) Electron tomography of the supramolecular structure of virus-infected cells. Curr Opin Struct Biol 20:632–639
59. Crowther RA, Amos LA, Finch JT, De Rosier DJ, Klug A (1970) Three dimensional reconstructions of spherical viruses by fourier synthesis from electron micrographs. Nature 226:421–425

Further Reading

Agbandje-McKenna M, McKenna R (eds) (2011) Structural virology. RSC Publishing, Cambridge
Jensen GJ (ed) (2010) Cryo-EM, Part A. Sample preparation and data collection. Methods in Enzymology, vol 481; Cryo-EM, part B. 3-D Reconstruction. Methods in Enzymology, vol 482; Cryo-EM, part C. Analysis, interpretation and case studies. Methods in Enzymology, vol 483. Academic Press
Rossmann MG, Rao VB (eds) (2012) Viral molecular machines. Adv Exp Med Biol, vol 726. Springer, New York

Also especially recommended for further reading are references [3, 4, 11, 23, 25, 26, 27, 35] *listed above*.